

Studies on the Wear and Corrosion Resistance of Ni-Fe-Co-P-GO Composite Coating Prepared by Scanning Electrodeposition

Xiu-qing Fu^{1, *}, Xiao-xin Shi¹, Shuang-lu Duan¹, Mo-qi Shen¹, Jin-ran Lin¹, Min-Jie Jiang¹

College of Engineering, Nanjing Agricultural University, Nanjing 210031, P. R. China

*E-mail: fuxiuqing@njau.edu.cn

Received: 14 January 2020 / Accepted: 19 March 2020 / Published: 10 June 2020

In order to improve the problem of unsatisfactory wear and corrosion resistance of traditional materials, a composite coating of Ni-Fe-Co-P-GO is prepared on the surface of 45# steel by scanning electrodeposition technology. The morphology, composition and phase structures of the Ni-Fe-Co-P-GO composite coatings are characterized by scanning electron microscopy (SEM), energy spectrum analysis (EDS) and X-ray diffractometry (XRD). The surface hardness, wear resistance and corrosion resistance of the composite coatings are analyzed by means of a micro hardness tester, a comprehensive tester for surface properties of materials and an electrochemical workstation. The results prove formation of an amorphous Ni-Fe-Co-P-GO composite coating on the surface of 45# steel. The prepared Ni-Fe-Co-P-(GO)_{0.6} composite coating has maximum surface hardness with best wear and corrosion resistance due to closely connected cell structure on the surface when the concentration of graphene oxide (GO) is 0.6 g·L⁻¹.

Keywords: Scanning electrodeposition; Ni-Fe-Co-P-GO composite coating; wear resistance; corrosion resistance

1. INTRODUCTION

With rapid development of industrial modernization, higher requirements are being put forward for the hardness, abrasion resistance and corrosion resistance of engineering materials [1-3]. It has been difficult for traditional Ni-based coating to meet the requirements of applications and various attempts have been made by different research groups to improve the overall performance of the coating by forming alloys via introduction of Fe [4], Cu [5], Mn [6], Co [7] and other elements [8-10] in the coating. Scanning electrodeposition technology is a computer-controlled technique where the motion track of nozzle and the switching on and off of the DC power supply of the electrode for electrodeposition is controlled by PC in order to complete the electrodeposition on the cathode surface. This technology is suitable for the preparation of composite coating [11-13] due to its various advantages like simple

process, low cost, faster deposition and higher efficiency.

Studies have shown that coating based on the Ni-Fe-Co-P quaternary alloy has higher hardness, good corrosion resistance, abrasion resistance, high temperature resistance and other excellent properties [14-16]. Composite coating having specific properties are prepared by the addition of insoluble second phase particle in the alloy coating for co-deposition with the matrix metal [17-20]. Graphene is a new type of carbon nanostructure with thickness of only a single atom, and is tightly packed with hexagonal carbon atom structure via sp^2 hybridization. Its excellent carrier properties are unmatched by ordinary second-phase materials in terms of mechanics and electricity. Due to the unique structure of graphene, the graphene composites prepared by traditional sintering process is vulnerable to damage. However, the graphene composites prepared by scanning electrodeposition can retain the structure of graphene and enhance the properties of the composites [21,22]. Graphene oxide (GO) as a kind of graphene oxide derivatives, due to the special structure of graphene is not easy to dissolve in water, not easy to do scientific research, graphene oxide becomes a substitute graphene, it exists in the structure of a large number of the epoxy groups and hydroxyl, carboxyl and hydrophilic group, make its highly hydrophilic, easily with other polymers to form new nanocomposites [23-25].

In the recent years, studies on Ni-based composite coatings have focused on the binary and ternary alloy coatings, and there is relatively little research on quaternary Ni-Fe-Co-P alloy coating. Graphene oxide (GO) as the second phase particle of the metal matrix composites has received very less attention. Based on this, this article adopts scanning electrodeposition technology of the preparation of coatings based on Ni-Fe-Co-P-GO composite, exploring the GO concentration effect (0, 0.2, 0.4, 0.6, 0.8 $g \cdot L^{-1}$) in the plating solution on the properties of the coating, along with the sedimentary principle of composite coating and thereby laying a foundation for the development of new composite materials.

2. EXPERIMENTAL

2.1. Test principle

The scanning electrodeposition test device used for the experimental study is shown in Figure 1. The system mainly consists of CNC machine tool, nickel rod as anode, nozzle, power supply unit, cathode material, electrodeposition tank, liquid tank containing electrolyte, temperature control unit, pump, flow meter and other components. During the test, the electrolyte is heated to an appropriate temperature in the liquid tank, and then pumped to the anode, and then sprayed on the cathode material surface at a certain velocity and pressure through the nozzle at the positive extreme. The motion track of the nozzle and switching on and off of the DC power supply of the electrodeposition electrode are controlled by the computer control system to complete the deposition on the cathode surface, in which the nozzle performs a linear reciprocating scanning motion in the X direction. Different from traditional electrodeposition, the cyclic flow of the plating solution accelerates the ion transmission, and at the same time, the deposition rate is greatly improved by increasing the limiting current density. The impact of the plating solution can mechanically activate the coating, making the coating grain fine, uniform and dense.

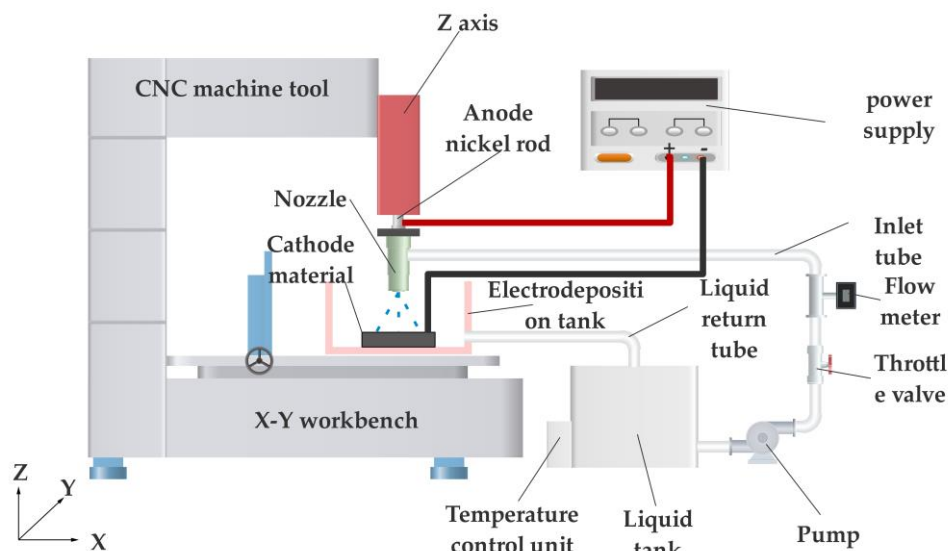


Figure 1. Schematic diagram of scanning electrodeposition test device.

2.2. Experimental

The anode material used in this experiment is pure Ni rod (99.9% purity), and the cathode material is 45# steel having dimension of 25 mm × 10 mm × 8 mm, whose composition is as per the Table 1. Details of the plating solution and experimental conditions are shown in Table 2. The graphene oxide (GO) used in the experiment (provided by Shenzhen Turing evolution technology co., LTD., China) is prepared by REDOX method [26], with a single-layer sheet diameter of 0.2-1 μm. GO particles in the range of 0~0.8 g·L⁻¹ are added to the above electroplating solution to obtain the final Ni-Fe-Co-P electroplating solution. In order to ensure the uniform suspension of the GO particles in the electrolyte, the solution should be continuously stirred. The reagent used is analytically pure and prepared with deionized water. The cathode workpiece is polished with water sandpaper of 800# and 1500# successively. Before processing, the workpiece is pretreated and activated according to the activation process shown in Figure 2. After each step, the workpiece is washed with deionized water. Finally, the workpiece is cleaned ultrasonication and blow-dried.

Table 1. Chemical composition of 45# steel.

| Element | C | Cr | Mn | Ni | P | S | Si |
|-------------|-----------|-------|-----------|-------|--------|--------|-----------|
| Content (%) | 0.42~0.50 | ≤0.25 | 0.50~0.80 | ≤0.25 | ≤0.035 | ≤0.035 | 0.17~0.37 |

Table 2. Composition of plating solution and experimental conditions.

| Sample name | Plating solution compositions and experimental conditions |
|-------------|---|
| Ni-Fe-Co-P | NiSO ₄ ·6H ₂ O (120 g·L ⁻¹) |
| | NiCl ₂ ·6H ₂ O (40 g·L ⁻¹) |
| | FeSO ₄ (20 g·L ⁻¹) |

| | |
|--------------------------------|---|
| | <p>CoSO₄ (10 g·L⁻¹) H₃PO₃(30 g·L⁻¹) H₃BO₃(30 g·L⁻¹) Citric acid (10 g·L⁻¹) Thiourea (0.01 g·L⁻¹) Sodium dodecyl sulfate (0.08 g·L⁻¹) pH:3.5 Operating time:20 min Current density:0.6 A Solution temperature:65°C</p> |
| Ni-Fe-Co-P-(GO) _{0.2} | Ni-Fe-Co-P +GO (0.2 g·L ⁻¹) |
| Ni-Fe-Co-P-(GO) _{0.4} | Ni-Fe-Co-P +GO (0.4 g·L ⁻¹) |
| Ni-Fe-Co-P-(GO) _{0.6} | Ni-Fe-Co-P +GO (0.6 g·L ⁻¹) |
| Ni-Fe-Co-P-(GO) _{0.8} | Ni-Fe-Co-P +GO (0.8 g·L ⁻¹) |

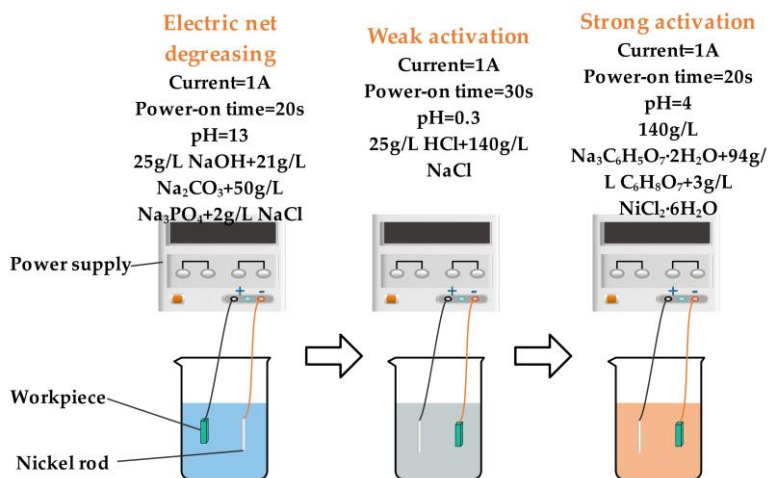


Figure 2. Activation process.

2.3 Instruments

The microstructure and composition of the composite coatings are observed by scanning electron microscopy (FEI-SEM, Quanta FEG250; FE Instruments, Oregon, USA) and EDS spectrum analyzer (XFlash 5030 Bruker AXS, Inc., Berlin, Germany), with the accelerating voltage of 20 kV; the phase structure of the coating is analyzed by X-ray diffractometer (PANalytical X'pert; PANalytical Inc.), having Cu target with wavelength of $\lambda=0.15406\text{\AA}$. During the XRD measurement, the accelerating voltage, applied current, scanning rate and scanning angles are 40 kV, 40 mA, 0.33 °/min, and 10°~90°, respectively. The microhardness of the coating surface is measured by a microhardness measuring instrument (Duramin-40; Struers, Denmark). The test load is 100 g, with 15 s being the load duration. The measurement is carried out five times and average of these measurements is taken as the output value. The friction and wear test are carried out on the CFT-I material surface performance

comprehensive tester (Lanzhou Zhongke Kaihua Technology); the OLYMPUS LEXT4100 laser confocal microscope (Olympus, Japan) is used to measure the surface wear scar of the coating. The polarization curve and impedance spectrum of the electrochemical workstation CS350 (Wuhan Corrtest Instruments Corp., Ltd., Wuhan, China) are measured by a three-electrode system. The corrosive medium is $50 \text{ g}\cdot\text{L}^{-1}$ NaCl solution, the scanning frequency of the polarization curve is $5 \text{ mV}\cdot\text{s}^{-1}$, and the scanning frequency range of the electrochemical impedance spectrum is $100 \text{ kHz} \sim 10 \text{ MHz}$, with the amplitude of the AC excitation signal being 5 mV .

3. RESULTS AND DISCUSSION

3.1. Morphology analysis of Ni-Fe-Co-P-GO composite coatings

Figure 3 shows the surface morphology of the prepared Ni-Fe-Co-P-GO composite coatings. It can be seen from Figure 3a that the surface of the Ni-Fe-Co-P alloy coating exhibits a cell structure, and the size of the cell structure is different with disordered arrangement. When the graphene oxide is added in the plating solution, the surface morphologies of the composite coatings change in varying degrees. Figure 3b and 3c show the surface morphology of the Ni-Fe-Co-P-GO composite coating having GO concentration of $0.2 \text{ g}\cdot\text{L}^{-1}$ and $0.4 \text{ g}\cdot\text{L}^{-1}$, respectively. The coating still shows a cell structure, but in comparison to the Ni-Fe-Co-P coating, part of the cell structure becomes larger and the filling is denser for the Ni-Fe-Co-P-GO composite. Figure 3d shows the surface morphology of the Ni-Fe-Co-P-GO composite coating with a GO concentration of $0.6 \text{ g}\cdot\text{L}^{-1}$. It can be observed that the cell surface structure of the coating layer is further enlarged, gradually filling the entire surface and the cell structures are dense and continuous, with no obvious defects such as pores and cracks. Figure 3e shows the surface morphology of the Ni-Fe-Co-P-GO composite coating with a GO concentration of $0.8 \text{ g}\cdot\text{L}^{-1}$ when the cell structure spacing becomes larger, the surface becomes rough, and there is obvious agglomeration. Figure 3f shows the EDS spectrum obtained by selective scanning of the Ni-Fe-Co-P-(GO)_{0.6} composite coating. Appearance of five peaks in the spectrum corresponding to the elements like Ni, Fe, Co, P and C indicate successful coating of the Ni-Fe-Co-P-GO composite on the surface of 45# steel. On the other hand, Figure 3g shows the elemental distribution with even distribution of each element which is obvious.

Figure 4 depicts the effect of GO particles on the deposition of Ni-Fe-Co-P-GO alloy coating. As shown in Figure 4a, the reduction of the metal ions takes place at the cathode. Since the deposition rate of the metal atoms is relatively fast, a large amount of H^+ ion is inevitably captured into the deposited layer [27], so that the surface of the plating layer is randomly stacked as shown in Figure 3a, resulting in defects such as bumps and pits. In Figure 4b, after the GO particles are added in the plating solution, the sheet-shaped GO particles serve as heterogeneous nucleation sites. The adsorbed metal ions preferentially nucleate and grow at the cathode, and the crystal nucleus grows into uniformly dispersed particles on the surface of the cathode [28]. At the same time, an effective diffusion channel of H^+ is formed, which promotes the evolution of hydrogen during the deposition process, and finally forms a Ni-Fe-Co-P-GO composite coating (Figure 3b,3c,3e). However, when the GO is excess, it is excessively adsorbed on the surface of the metal substrate, causing the surface-active sites of the substrate to be

masked and lose activity. Subsequently, the nucleation sites are greatly reduced or even inhibited, resulting in the formation of a larger bulge via uneven particle agglomeration deposits on the surface of the plating layer. Thus, the quality of the coating is affected (Figure 3e), and the obvious advantage of GO is lost [29].

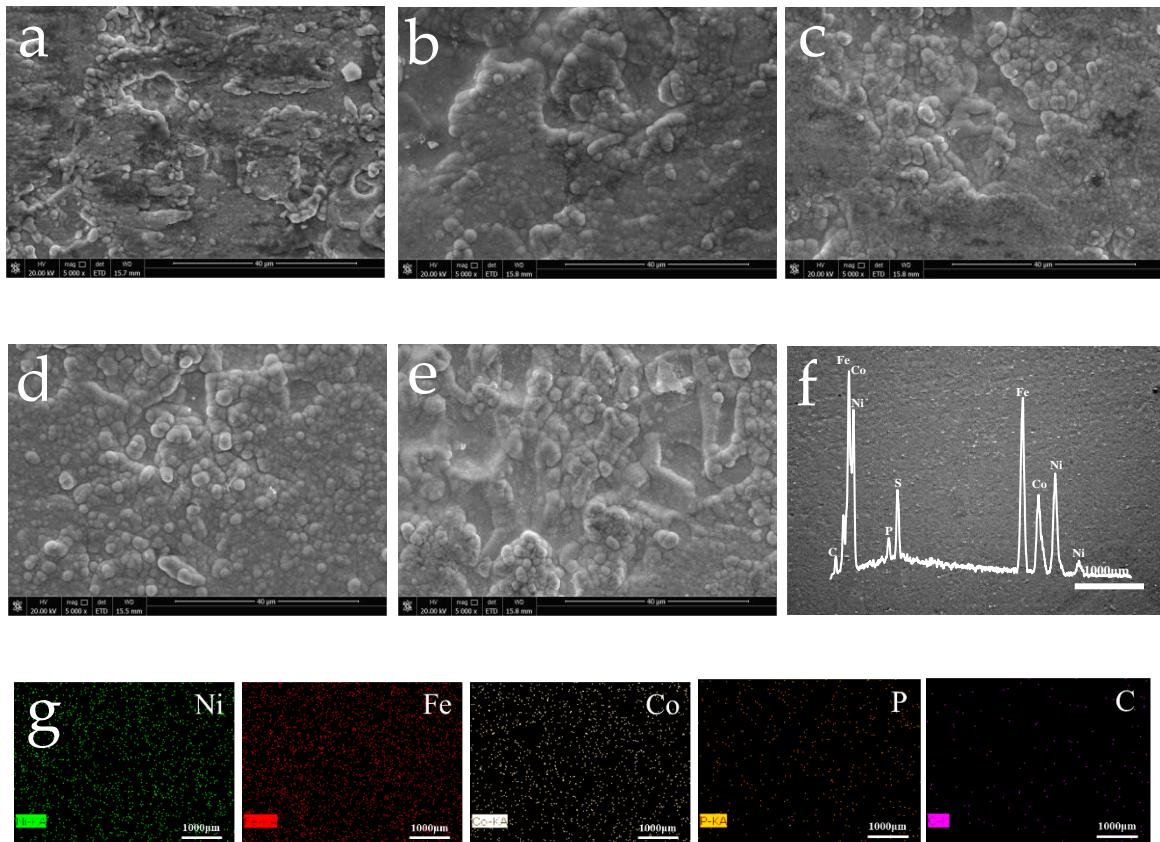


Figure 3. SEM images of composite coatings: (a) Ni-Fe-Co-P; (b) Ni-Fe-Co-P-(GO)_{0.2}; (c) Ni-Fe-Co-P-(GO)_{0.4}; (d) Ni-Fe-Co-P-(GO)_{0.6}; (e) Ni-Fe-Co-P-(GO)_{0.8}; (f) EDS spectrum of Ni-Fe-Co-P-(GO)_{0.6} composite coating and (g) Element map of Ni-Fe-Co-P-(GO)_{0.6} composite coating.

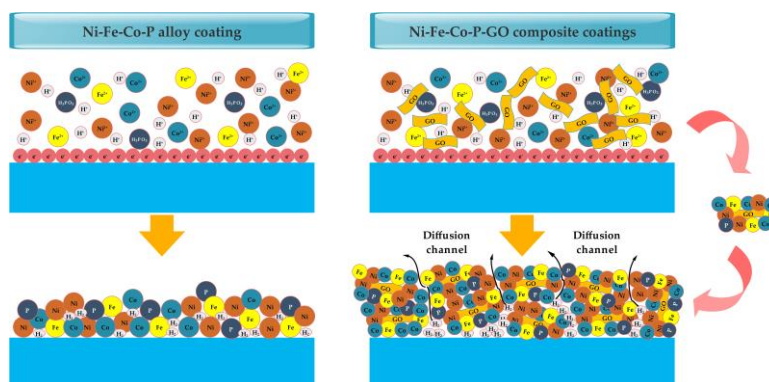


Figure 4. Schematic diagram of deposition principle of Ni-Fe-Co-P-GO composite coatings.

3.2 Microstructure analysis of Ni-Fe-Co-P-GO composite coatings

Figure 5 shows XRD patterns of the five Ni-Fe-Co-P-GO composite coatings. By observing the XRD patterns, it can be seen that the Ni-Fe-Co-P alloy coatings show relatively sharp diffraction peaks, indicating that the coatings of the Ni-Fe-Co-P alloy without GO are crystal superposition mixed structures, that is, microcrystalline structures. On the other hand, the Ni-Fe-Co-P-GO composite coatings with GO show no obvious sharp diffraction peaks, and appearance of broad gimmick peaks on the Ni (111) plane ($2\theta = 45^\circ$), indicates that these composite coatings are having amorphous structure. By combining the XRD patterns of the five Ni-Fe-Co-P-GO composite coatings and the content of each element in the coating, the crystal structure of the coating has evolved from being microcrystalline in the Ni-Fe-Co-P alloy coating to amorphous in the Ni-Fe-Co-P-GO composite coating. This is because the phase composition of the Ni-Fe-Co-P alloy coating is largely determined by the content of Phosphorus (P) in the coating. At the same time, with the increase of GO concentration, it is found that the X-ray diffraction peak becomes a gentler peak of steamed buns, and the degree of diffraction decreases more slowly within a wide diffraction angle, which is a sign of higher amorphous coating. The content of the element P in the Ni-Fe-Co-P-GO composite coating is shown in the Table 3. The P content changes linearly with the change in the concentration of the graphene oxide, with subsequent gradual increase in the degree of amorphization of the coating. Graphene oxide has a large specific surface area and strong adsorption capacity, and can adsorb more HPO_3^{2-} to its surroundings to form an HPO_3^{2-} rich region, thereby allowing more elemental P to be deposited in the plating layer. The increase in the degree of amorphousness of the plating layer with increasing GO concentration is consistent with the results in the literature [30,31].

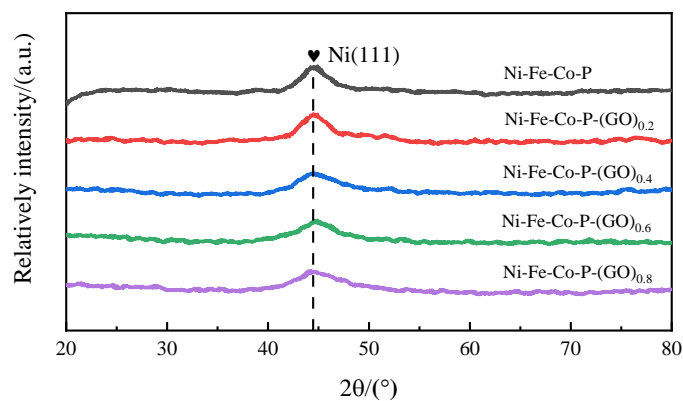


Figure 5. XRD pattern of Ni-Fe-Co-P-GO composite coatings.

Table 3. Element P content of Ni-Fe-Co-P-GO composite coating.

| Sample | Ni-Fe-Co-P | Ni-Fe-Co-P-(GO) _{0.2} | Ni-Fe-Co-P-(GO) _{0.4} | Ni-Fe-Co-P-(GO) _{0.6} | Ni-Fe-Co-P-(GO) _{0.8} |
|-------------|------------|--------------------------------|--------------------------------|--------------------------------|--------------------------------|
| Content (%) | 2.24 | 2.43 | 2.98 | 3.34 | 3.61 |

3.3 Microhardness analysis of Ni-Fe-Co-P-GO composite coatings

The microhardness of the 45# steel matrix is measured to be 153.83 HV_{0.1}. The effect of different concentrations of GO on the microhardness of the Ni-Fe-Co-P-GO composite coating is shown in Figure 6. As the GO concentration increased, the average microhardness of the composite coating shows an initial increasing trend followed by subsequent decrease. Maximum average microhardness value of 638.83 HV_{0.1} for the composite coating is achieved for subsequent GO concentration of 0.6 g·L⁻¹ which is nearly 47 % higher than that of the pure Ni-Fe-Co-P alloy coating (434.85 HV_{0.1}). According to the results, in addition to the self-lubrication of GO itself and its special mechanical properties, the microstructure of the composite coating is also strengthened [32]. When the content of GO is increased from 0 g·L⁻¹ to 0.6 g·L⁻¹, the surface of GO is in contact with the surface of the substrate. When the number of active particles increases, the chance of adsorption between them increases, resulting in an increase in the content of the second phase particles of GO in the composite coating. Hence so that the composite coating gains the advantage of solid solution strengthening and grain refinement, thereby increasing the microhardness. When the content of GO is 0.8 g·L⁻¹, agglomeration tends to occur, and the quality of the Ni-Fe-Co-P-GO composite coating deteriorates, resulting in the decrease of the microhardness.

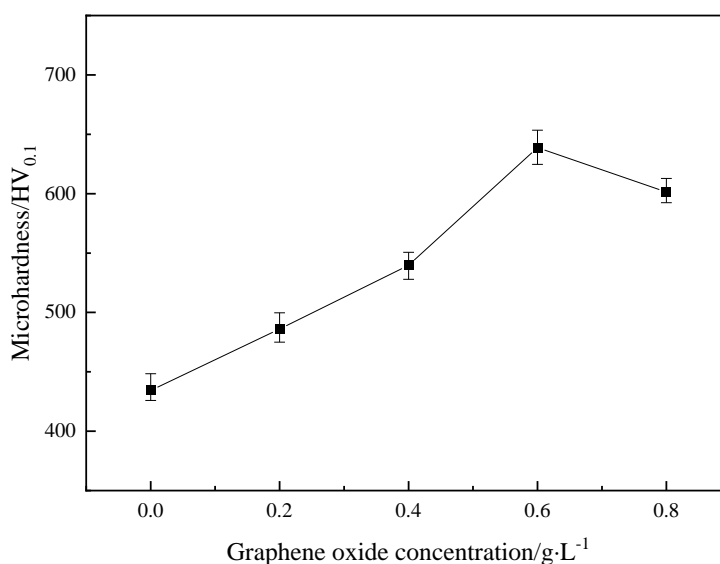


Figure 6. Microhardness curve of Ni-Fe-Co-P-GO composite coatings.

3.4 Wear resistance analysis of Ni-Fe-Co-P-GO composite coatings

The friction and wear test on the material surface performance were carried out using comprehensive tester. The GCr15 grinding ball with a diameter of 5 mm was used to trace back and forth on the surface of the coating for 20 min. The length of the wear scar is 4 mm with 320 g load. The principle of the friction and wear test is shown in Figure 7. Figure 7 also shows the friction coefficient curve of Ni-Fe-Co-P-GO the composite coating. It can be found that the friction coefficient curve of the composite coating first goes through a running-in phase and then tends to a stable value because the

abrasion resistance test is performed on the surface of the unpolished coating.

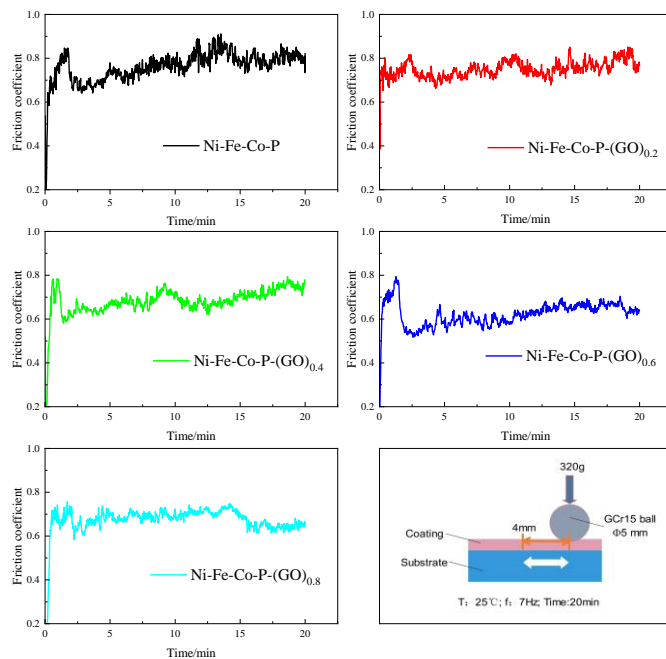
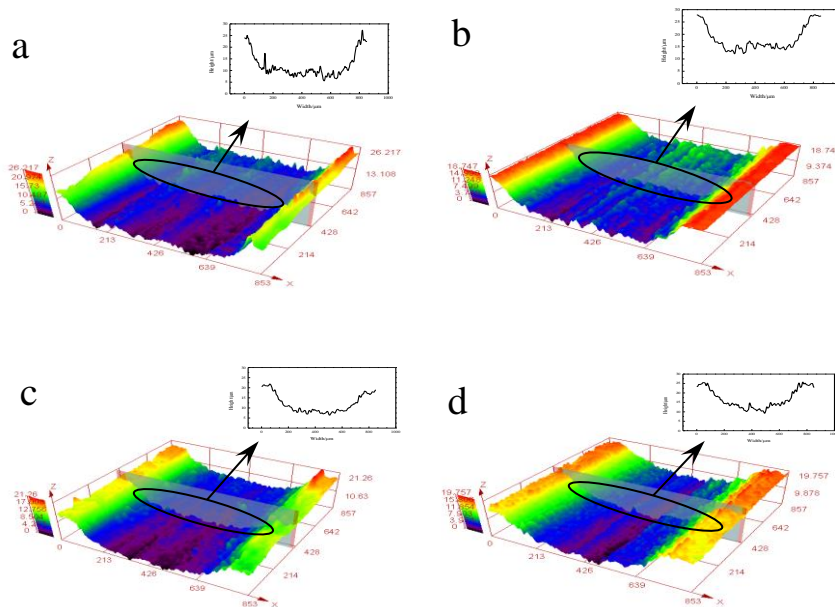


Figure 7. Friction coefficient curve of Ni-Fe-Co-P-GO composite coatings.



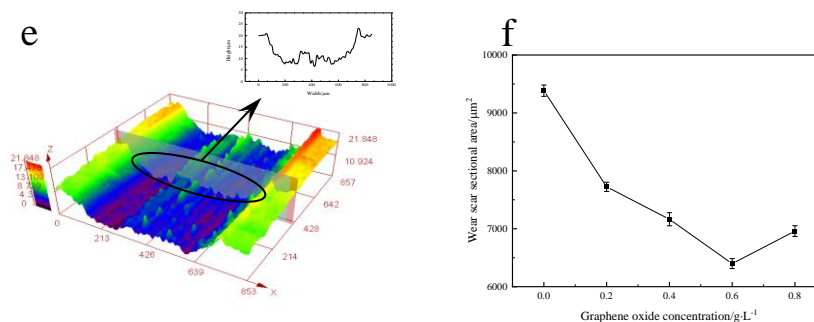


Figure 8. Wear profile and wear section parameters of composite coatings: (a) Ni-Fe-Co-P; (b) Ni-Fe-Co-P-(GO)_{0.2}; (c) Ni-Fe-Co-P-(GO)_{0.4}; (d) Ni-Fe-Co-P-(GO)_{0.6}; (e) Ni-Fe-Co-P-(GO)_{0.8} and (f) The curve of wear scar sectional area.

At the beginning, there is a certain roughness between the surfaces of the coating and load pairs, so the coefficient of friction is large. As the friction process progresses, the pairs are fully meshed together (this process is generally short), and consequently the friction coefficient drops to a substantially stable value. When the friction is stable the friction coefficient decreases first and then increases with the increase of GO concentration. The minimum value of 0.6 for friction coefficient is achieved for GO concentration of 0.6 g·L⁻¹. Figure 8 shows the cross-sectional morphology and parameters of the Ni-Fe-Co-P-GO composite coating after the friction and wear test. It can be seen that with the increase of GO concentration, the cross-sectional area of the wear scar decreases, reaching the smallest cross-sectional area when the GO concentration is 0.6 g·L⁻¹ followed by subsequent rise (Figure 8f). Under the same wear scar length, the cross-sectional area of the wear scar is small, the wear amount is small, and the wear resistance is good. It can be seen that when the GO concentration is 0.6 g·L⁻¹, the composite coating has the best wear resistance.

Figure 9 is the SEM pictures of the wear scar of the Ni-Fe-Co-P-GO composite coatings at different GO concentration. As can be seen from Figure 9a that there is a large area of adhesion and peeling on the surface of the wear scar, indicating that there is adhesive wear for the Ni-Fe-Co-P coating. It is found in the Figures 9b, 9c, 9d that the wear scar has a shallow furrow along the rubbing direction, and the adhesion is not obvious, so the main wear form of the coating is abrasive wear. Although the wear scar pattern is obtained in the intense wear stage, the surface of the wear scar is smooth after adding appropriate amount of the graphene oxide particles, and there is no large-scale adhesion and peeling phenomenon. This is due to the fact that specific surface area of the graphene oxide is large, thereby reducing the coating layer and adhesive for grinding parts. Subsequently, the anti-adhesion ability of the coating along with the surface toughness is improved. It also results in the reduction of the lubricating effect of the graphene oxide, shear stress on the coating of the grinding member, the surface plastic deformation, and the contact fatigue wear [33]. However, addition of excess amount of graphene oxide particles (Figure 9e) lowers the surface quality of the plating layer. The abrasive member and the plating layer are pressed and rubbed against each other, thus breaking the plating layer and generating wear debris. As time passes, the wear debris increases and fatigue wear occurs.

The reasons for the above-mentioned changes in the friction and wear properties of the coating are as follows: On the one hand, the wear resistance is closely related to the hardness [34] and the

increase in hardness can greatly reduce the abrasive wear and adhesive wear of the coating, thereby improving the wear resistance. The same verification was obtained in Lee's research [35]. On the other hand, GO, with high hardness and good lubrication as a second-phase hard particle can well support the structure of the coating, and improves the resistance to deformation of the coating, thereby improving the abrasion resistance of the coating [36].

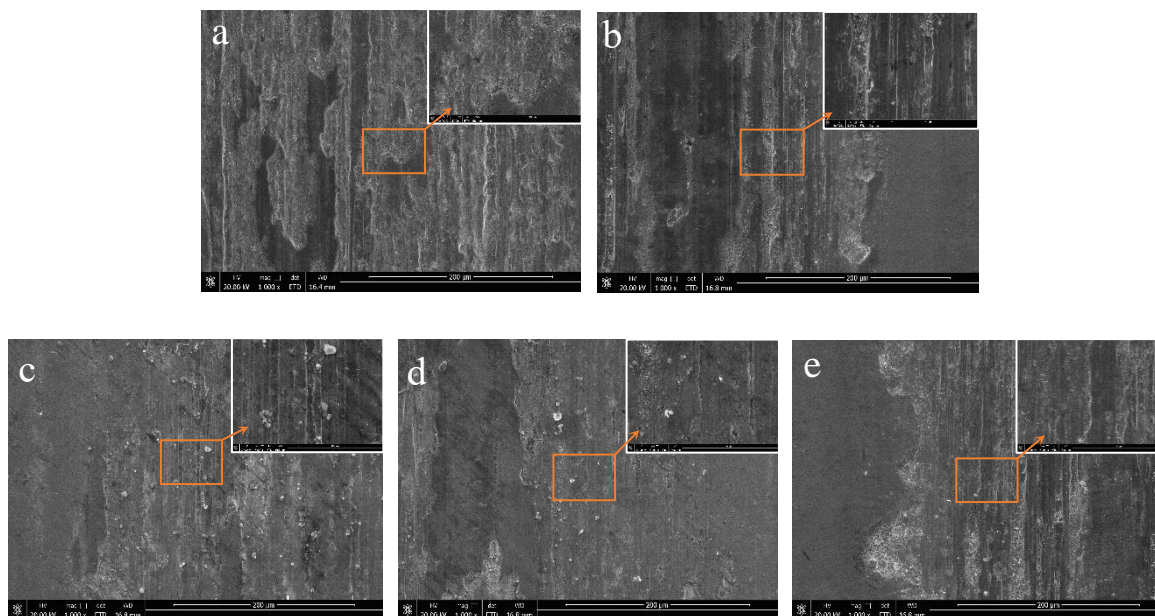


Figure 9. SEM image of wear scar of composite coatings: (a) Ni-Fe-Co-P; (b) Ni-Fe-Co-P-(GO)_{0.2}; (c) Ni-Fe-Co-P-(GO)_{0.4}; (d) Ni-Fe-Co-P-(GO)_{0.6}; (e) Ni-Fe-Co-P-(GO)_{0.8}.

3.5 Corrosion resistance analysis of Ni-Fe-Co-P-GO composite coatings

The corrosion behavior of the Ni-Fe-Co-P-GO composite coatings with different GO concentrations is studied in presence of 50 g·L⁻¹ NaCl solution. The corresponding potentiodynamic polarization curves are shown in Figure 10. The relevant parameters of the potentiodynamic polarization curves are fitted with the obtained self-corrosion potential (E_{corr}), self-corrosion current (I_{corr}) and corrosion rate (CR) are listed in Table 4, where B_a is the anode polarization slope and B_c is the cathode polarization slope. Referring to Figure 10 and Table 4, the self-corrosion potential (E_{corr}) of the Ni-Fe-Co-P coating is -0.829V, and the self-corrosion current (I_{corr}) is 1.3395×10^{-5} A·cm⁻². The coating of the added GO has a positive transition for the corrosion potential, and the gradually decrease of the self-corrosion current indicates that the corrosion resistance of the coating is enhanced. When the concentration of GO is 0.6 g·L⁻¹, the self-corrosion potential (E_{corr}) of the coating is the largest (-0.303 V) compared with that of the Ni-Fe-Co-P alloy coating, and the self-corrosion current (I_{corr}) is also reduced to the minimum (0.9378×10^{-5} A·cm⁻²). When the GO content exceeds this value, the surface quality of the coating deteriorates, and the self-corrosion potential (E_{corr}) negatively migrates, and the self-corrosion current (I_{corr}) and the corrosion rate (CR) also increase, indicating that the corrosion

resistance is lowered. The asymmetric potentiodynamic polarization curves, that is, the unequal Tafel constant ($|Ba| \neq |Bc|$) indicates that the metal is corroded. As the GO concentration increases, the value of $|Ba|$ is higher than $|Bc|$, indicating that the anodic polarization causes corrosion.

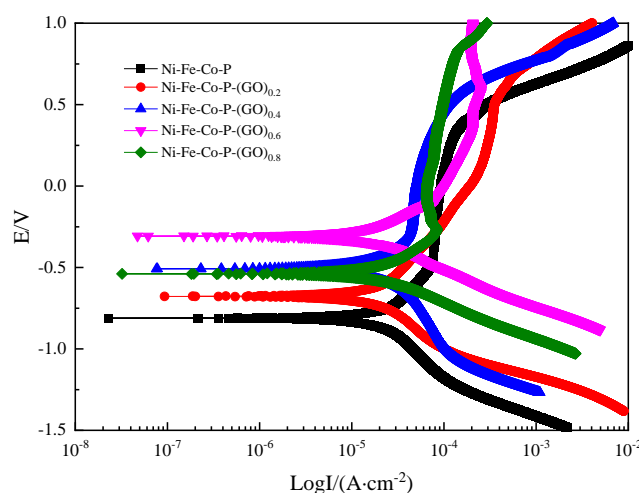


Figure 10. Potentiodynamic polarization curves of Ni-Fe-Co-P-GO composite coatings at scanning rate of $5\text{mV}\cdot\text{s}^{-1}$.

Table 4. Polarization curve parameter value of Ni-Fe-Co-P-GO composite coatings.

| Sample | Ba(mV) | Bc(mV) | $I_{\text{corr}}(\text{A}\cdot\text{cm}^{-2})$ | $E_{\text{corr}}(\text{V})$ | CR ($\text{mm}\cdot\text{a}^{-1}$) |
|--------------------------------|--------|--------|--|-----------------------------|--------------------------------------|
| Ni-Fe-Co-P | 423 | -336 | 1.3395×10^{-5} | -0.829 | 0.202 |
| Ni-Fe-Co-P-(GO) _{0.2} | 350 | -266 | 1.2693×10^{-5} | -0.682 | 0.153 |
| Ni-Fe-Co-P-(GO) _{0.4} | 270 | -240 | 1.0798×10^{-5} | -0.508 | 0.139 |
| Ni-Fe-Co-P-(GO) _{0.6} | 188 | -157 | 0.9378×10^{-5} | -0.303 | 0.113 |
| Ni-Fe-Co-P-(GO) _{0.8} | 280 | -182 | 1.4382×10^{-5} | -0.544 | 0.174 |

In order to further characterize the corrosion resistance of the composite coating, the electrochemical impedance spectroscopy (EIS) is carried out in this work. Figure 11 shows the AC impedance spectra of the coatings obtained at different scanning frequencies. The values of the parameters after fitting with the equivalent circuit diagram are shown in Table 5. R_s represent the resistance in solution, R_{ct} represents the charge transfer resistance, CPE represents the constant phase angle element, and its impedance is

$$Z = \frac{1}{Y_0(j\omega)^{-n}}$$

Where, Y_0 is a tunable parameter (for nonlinear least squares fitting), n value is between 0~1, (for ideal capacitance $n=1$ and for ideal resistance $n=0$), CPE component is the pure resistance [37]. The corrosion resistance of the Ni-Fe-Co-P-GO composite coating is analyzed in combination with Figure 11 and Table 5. It is obvious that the capacitive arc radius of the Ni-Fe-Co-P-GO composite coatings are larger than that of the pure Ni-Fe-Co-P alloy coating, and the radius of the capacitive arc is used as the

characterization of the electrochemical corrosion behavior of the coating. Larger the value of the capacitive arc, the stronger is the corrosion resistance of the coating. It can be directly seen from Table 5 that the addition of GO reduces the polarization resistance R_{ct} of the composite plating layer, the corrosion tendency of the plating layer in the NaCl solution is lowered, and when the GO concentration is $0.6 \text{ g}\cdot\text{L}^{-1}$, compared with the other plating layers. The charge transfer resistance (R_{ct}) calculated by Zview software is the largest ($1284 \text{ }\Omega\cdot\text{cm}^{-2}$), indicating that the transfer of charge between the solution and the electrode has the greatest hindrance and is not easily corroded, indicating that the introduction of GO can effectively improve the corrosion resistance of the coating.

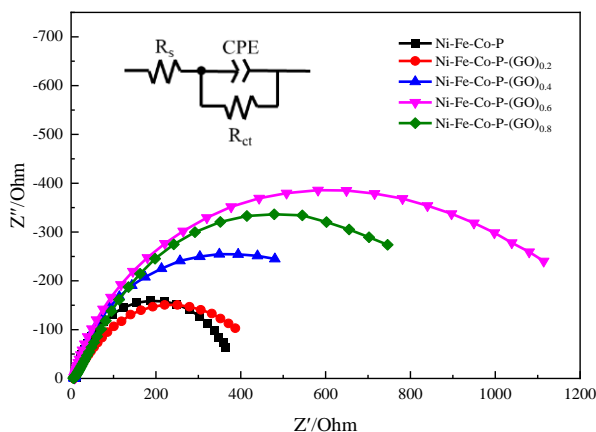


Figure 11. Electrochemical impedance spectroscopy (EIS) of Ni-Fe-Co-P-GO composite coatings at the scanning frequency range of 100 kHz~10 MHz.

Table 5. Equivalent circuit diagram parameter value of Ni-Fe-Co-P-GO composite coatings.

| Sample | $R_s(\Omega\cdot\text{cm}^{-2})$ | $\text{CPE-T}(\text{F}\cdot\text{cm}^{-2})$ | CPE-P | $R_{ct}(\Omega\cdot\text{cm}^{-2})$ | Error (%) |
|--------------------------------|----------------------------------|---|---------|-------------------------------------|-----------|
| Ni-Fe-Co-P | 11.23 | 2.8178×10^{-5} | 0.89369 | 375.7 | 1.4 |
| Ni-Fe-Co-P-(GO) _{0.2} | 6.334 | 138.62×10^{-5} | 0.67519 | 518.7 | 1.7 |
| Ni-Fe-Co-P-(GO) _{0.4} | 7.72 | 8.6575×10^{-5} | 0.835 | 658.5 | 1.2 |
| Ni-Fe-Co-P-(GO) _{0.6} | 7.923 | 4.5905×10^{-5} | 0.8082 | 1284 | 1.6 |
| Ni-Fe-Co-P-(GO) _{0.8} | 6.368 | 114.22×10^{-5} | 0.65565 | 1022 | 5.1 |

In summary, addition of an appropriate amount of GO to the plating solution can improve the corrosion resistance of the coating, and the lifting effect is best when the GO concentration is $0.6 \text{ g}\cdot\text{L}^{-1}$. The reason is that graphene oxide has high chemical and thermal stability, and can form a stable physical

barrier layer between the active medium and the metal matrix, thereby effectively blocking the passage of other substances such as oxygen, water and chloride ions [38]. The high conductivity of the GO sheet layer can also hinder the electron transfer during the corrosion process and slow down the corrosion [39]. The increased concentration of the element P provided by the reducing agent in the surface of the coating makes the coating more amorphous and as is well known, the amorphous materials have good corrosion resistance in the medium. A protective film prevents corrosion, which is also an important reason for the change in the corrosion resistance of the coating with the change in the content of the graphene oxide [40]. As the concentration of graphene oxide continues to increase, too large concentration of graphene oxide in the plating solution results in weakened collision between the ions and easy agglomeration, causing the coating to become rough, and have poor flatness and brightness. The quality of Ni-Fe-Co-P-GO the composite coating is reduced and the corrosion resistance is lowered.

4. CONCLUSIONS

Ni-Fe-Co-P-GO composite coating is successfully prepared on the surface of 45# steel by scanning electrodeposition technology. The effect of graphene oxide (GO) concentration on the micromorphology, chemical composition and microstructure of the composite coating is studied. The abrasion and corrosion resistance properties are characterized.

(1) The GO of the layered structure has a positive influence on the microstructure and composition of the coating. The prepared Ni-Fe-Co-P-GO composite coating has an amorphous structure. Compared with the corresponding Ni-Fe-Co-P alloy coating, the Ni-Fe-Co-P-GO composite coating has a larger surface cell structure, some cauliflower-like structures with smaller nodules, and the pore structure is uniform and dense.

(2) The appropriate amount of GO can improve the mechanical properties and wear properties of the coating. When the GO concentration is $0.6 \text{ g}\cdot\text{L}^{-1}$, the Ni-Fe-Co-P-(GO)_{0.6} composite coating has the best wear resistance, with a microhardness value of 638.83 HV_{0.1} and a friction coefficient of 0.6, and the cross-sectional area of the wear scar is also the smallest. At the same time, abrasive wear occurs on the surface of the coating, and the wear resistance is significantly improved.

(3) An appropriate amount of GO can improve the corrosion resistance of the coating. When the GO concentration is $0.6 \text{ g}\cdot\text{L}^{-1}$, the prepared Ni-Fe-Co-P-(GO)_{0.6} composite coating has the best corrosion resistance, showing a higher self-corrosion potential ($E_{\text{corr}} = -0.303 \text{ V}$), a lower self-corrosion current ($I_{\text{corr}} = 0.9378 \times 10^{-5} \text{ A}\cdot\text{cm}^{-2}$) and larger charge transfer resistance ($R_{\text{ct}} = 1284 \text{ }\Omega\cdot\text{cm}^{-2}$).

ACKNOWLEDGEMENTS

Financial support for this work was provided by the China Postdoctoral Science Foundation (Grant number 2017M621665), the Postdoctoral Science Foundation of Jiangsu Province of China (Grant number 2018K022A), National College Student Innovation Training Program (Grant number 201910307079Z) and Nanjing Agricultural University Innovation Training Plan (Grant number 1930A49).

References

1. H. Li, M. Kang, Y. Zhang, Y. Liu, M. Jin, N. S. Mbugua, G. Zhu and C. Liu, *Coatings*, 9 (2019) 50.
2. I. Matsui, M. Kanetake, H. Hosokawa, N. Omura, Y. Takigawa and K. Higashi, *Mater. Trans.*, 59 (2018) 1354.
3. J. A. Cabral-Miramontes, D. M. Bastidas, M. A. Baltazar, P. Zambrano-Robledo, J. M. Bastidas Rull, F. M. Almeraya-Calderón and C. Gaona-Tiburcio, *Int. J. Electrochem. Sci.*, 21 (2019) 4226.
4. M. Scendo and K. Szczerba, *Int. J. Electrochem. Sci.*, 14 (2019) 1009.
5. B. Li, T. Mei, D. Li, S. Du, *Ultrason. Sonochem.*, 58 (2019) 104680.
6. Y. Shao, P. Y. Guo, H. Sun, T. C. Zhou, J. T. Ding, K. X. Xu, Y. X. Wang, Y. X. Guo and D. P. Wang, *J. Alloy. Compd.*, 811 (2019) 152006.
7. B. Li, W. Zhang and D. Li, *J. Alloy. Compd.*, 821 (2019) 153258.
8. G. B. Darband, M. Aliofkhaezraei, S. Hyun and A. S. Rouhaghdam, *Nanoscale*, 11 (2019) 16621.
9. W. Zhang, C. Ji and B. Li, *Results Phys.*, 13 (2019) 102242.
10. W. Dai, L. Lin, Y. Li, F. Li and L. Chen, *Int. J. Hydrogen Energy*, 44 (2019) 28746.
11. Z. Wang, L. Shen, W. Jiang, M. Fan, D. Liu and J. Zhao, *Surf. Coat. Technol.*, 377 (2019) 124886.
12. L. Shen, M. Xu, W. Jiang, M. Qiu, M. Fan, G. Ji and Z. Tian, *Appl. Surf. Sci.*, 489 (2019) 25-33.
13. Z. Wang, L. Shen, M. Qiu, W. Jiang, Y. Chen and J. Zhao, *Mater. Res. Express*, 6 (2019) 106409.
14. X. Fu, W. Ma, S. Duan, Q. Wang and J. Lin, *Materials*, 12 (2019) 2614.
15. D. H. Kim, S. Jo, J. Kwon, S. Lee and K. Eom, *Int. J. Hydrogen Energy*, 44 (2019) 15228-15238.
16. L. Pan, Y. He, M. Niu, Y. Dan and W. Li, *RSC Adv.*, 9 (2019) 21175-21185.
17. F. Xia, Q. Li, C. Ma, W. Liu and Z. Ma, *Ceram. Int.*, 46 (2020) 7961-7969.
18. F. Xia, Q. Li, C. Ma and X. Guo, *Ceram. Int.*, 46 (2020) 2500-2509.
19. K. O. Nayana, S. Ranganatha and H. N. Shubha, *Trans. Nonferrous Met. Soc. China*, 29 (2019) 2371-2383.
20. L. Xu, H. Wang, J. Gao and X. Jin, *J. Alloy. Compd.*, 809 (2019) 151802.
21. S. M. Kim, W. Kim, Y. Hwangbo, J. H. Kim and S. M. Han, *2d Materials*, 6 (2019) 045051.
22. N. Lotfi, T. Shahrabi, Y. Yaghoubinezhad and G. B. Darband, *Electrochim. Acta*, 326 (2019) 134949.
23. C. M. P. Kumar and T. V. Venkatesha, *Mater. Res. Bull.*, 48 (2013) 1477-1483.
24. M. A. Karimi and F. Banifateme, *J. Mater. Sci.: Mater. Electron.*, 28 (2017) 1844-1851.
25. M. H. Nazir, Z. A. Khan, A. Saeed, V. Bakolas, W. Braun, R. Bajwa and S. Rafique, *Materials (Basel, Switzerland)*, 10 (2017) 1225.
26. M. Y. Rekha, A. Kamboj and C. Srivastava, *Thin Solid Films*, 653 (2018) 82-92.
27. B. S. Li, Y. X. Huan and W. Zhang, *Surf. Eng.*, 35 (2019) 110-120.
28. X. H. Zhang, X. X. Li, W. J. Liu, Y. Q. Fan, H. Chen and T. X. Liang, *Rare Met.*, 38 (2019) 695-703.
29. G. Jin, D. Zhang, M. Liu, X. Cui, E. Liu, Q. Song, C. Yuan, X. Wen and Y. Fang, *J. Alloy. Compd.*, 801 (2019) 40-48.
30. C. Liu, D. Wei, X. Huang, Y. Mai, L. Zhang, and X. Jie, *J. Mater. Res.*, 34 (2019) 1726-1733.
31. H. Wu, F. Liu, W. Gong, F. Ye, L. Hao, J. Jiang and S. Han, *Surf. Coat. Technol.*, 272 (2015) 25-32.
32. Y. R. Dong, W. C. Sun, X. J. Liu, Z. W. Jia, F. Guo, M. Ma and Y. Y. Ruan, *Surf. Coat. Technol.*, 359 (2019) 141-149.
33. J. Chen, J. Li, D. Xiong, Y. He, Y. Ji and Y. Qin, *Appl. Surf. Sci.*, 361 (2016) 49-56.
34. W. Zhang, B. Li and C. Ji, *Ceram. Int.*, 45 (2019) 14015-14028.
35. L. Chun-Ying, M. Wei-Ti, G. Ming-Der and L. Hung-Bin, 366 (2019) 286-295.
36. Y. R. Dong, W. C. Sun, X. J. Liu, Z. W. Jia, F. Guo, M. Ma and Y. Y. Ruan, *Surf. Coat. Technol.*, 359 (2019) 141-149.
37. J. Jiang, C. Feng, W. Qian, L. Zhu, S. Han and H. Lin, *Mater. Chem. Phys.*, 199 (2017) 239-248.

38. J. Wang, W. Lei, Y. Deng, Z. Xue, H. Qian, W. Liu and X. Li, *Surf. Coat. Technol.*, 358 (2019) 765-774.
39. B. Wang, Y. Ma, C. Ran, G. Liu and Z. Hou, *Int. J. Electrochem. Sci.*, 14 (2019) 1884-1896.
40. A. Farzaneh, M. Mohammadi, M. Ehteshamzadeh and F. Mohammadi, *Appl. Surf. Sci.*, 276 (2013) 697-704

© 2020 The Authors. Published by ESG (www.electrochemsci.org). This article is an open access article distributed under the terms and conditions of the Creative Commons Attribution license (<http://creativecommons.org/licenses/by/4.0/>).